Applied Catalysis B: Environmental 179 (2015) 61–68

Contents lists available at ScienceDirect

Applied Catalysis B: Environmental

journal homepage: www.elsevier.com/locate/apcatb

$AgSbS_2$ modified ZnO nanotube arrays for photoelectrochemical water splitting

Jianhua Han, Zhifeng Liu*, Keying Guo, Xueqi Zhang, Tiantian Hong, Bo Wang

School of Materials Science and Engineering, Tianjin Chengjian University, 300384 Tianjin, China

ARTICLE INFO

Article history:
Received 1 March 2015
Received in revised form 5 May 2015
Accepted 5 May 2015
Available online 6 May 2015

Keywords:
$AgSbS_2$
ZnO
Nanotube
Photoelectrochemical
Water splitting

ABSTRACT

Large-scale, vertically aligned $AgSbS_2$ modified ZnO nanotube arrays have been fabricated directly on conducting glass substrates (ITO) via a facile, versatile and low-cost hydrothermal chemical process by using ZnO nanorods as reactive templates. This method is easy to be controlled to develop uniform morphology, and it can be generalized to fabricate other ternary sensitizer nanomaterial for PEC water splitting. In this work, we present a novel ternary sensitizer miargyrite $AgSbS_2$ for optimized ZnO, and the ZnO/$AgSbS_2$ nanoarrays film was applied on photoelectrochemical (PEC) photoelectrodes. Strikingly, the photocurrent density of this electrode was up to 5.08 mA cm^{-2} at 0.096 V versus Ag/AgCl. The excellent PEC properties stems from the enhanced absorption spectrum, high speed of photo-induced charges transmission velocity and appropriate energy gap of coupled nanostructures. Furthermore, this work demonstrates a promising low-cost method for preparing ternary sensitizer modified ZnO nanoarrays as PEC electodes for hydrogen production by water splitting.

1. Introduction

As a sustainable, renewable and clean energy, hydrogen energy is considered for an ideal candidate for instead of the traditional fossil energy in view of the growing crisis from energy and environment issues [1–3]. In the past decades, the development and application of hydrogen technologies have received considerable attention due to its intrinsic properties such as carbon-free and high gravimetric energy [4–5]. Among all the methods to manufacture hydrogen, PEC water splitting into hydrogen by semiconductor photoelectrodes is one of the most promising and eco-friendly methods [6–9]. Since the first report on water splitting using TiO_2 photoelectrode by Fujishima and Honda, metal oxides (such as ZnO, TiO_2 and Fe_2O_3) have been intensively investigated as photoelectrodes in PEC system because of their low cost and easy availability [10–13]. The PEC performance of metallic oxide-based photoelectrodes was significantly related to its morphology and structure [14]. Zinc oxide, ZnO, is an important photoelectric semiconductor material due to its simply synthesized to multifarious nanostructures and its extremely fast electron transmission rate [15–16]. Of particular interest are one-dimensional (1D) ZnO nanostructures (such as nanowires [17], nanotubes [18] and nanorods [19]), which provide a direct electrical pathway for electron transmission that can promote photo-induced electrons transport and reduce the recombination of carriers [20–21]. Nevertheless, one of the major drawbacks that ZnO-based photoelectrodes suffer from is only the UV fraction can be absorbed on account of the wide band-gap of ZnO, which restricts its practical applications [22].

In order to solve the aforementioned problem, many efforts have been put to broaden the adsorption spectrum of ZnO, including elemental doping and coupling with narrow band-gap semiconductors etc. [23–24]. Among these techniques, an efficient way is to deposit a sensitizer with appropriate band gap on ZnO. Silver antimony sulfide ($AgSbS_2$, Miargyrite), which has a suitable band gap (1.72 eV) according with the visible light region and a high absorption coefficient ($\alpha \sim 10^5$ cm^{-1}), has attracted great interest [25–26]. However, to our best knowledge, there has been no report on PEC electrodes of one-dimensional ZnO nanoarrays modified with ternary $AgSbS_2$ so far, this study extends the work to a new coupled semiconductor of ternary sensitizer $AgSbS_2$ decorated ZnO nanoarrays.

Motivated by the above concerns, we have successfully fabricated a coupled semiconductor based on $AgSbS_2$ modified ZnO nanoarrays through a simple hydrothermal chemical process. The hydrothermal chemical method is inexpensive, facile and eco-friendly. In addition, the ZnO/$AgSbS_2$ nanotube arrays were demonstrated to exhibit enhanced PEC activity in hydrogen evolution from water splitting. In this study, ternary $AgSbS_2$ sensitizer

* Corresponding author. Tel.: +86 22 23085236; fax: +86 22 23085110.
E-mail address: tjulzf@163.com (Z. Liu).

http://dx.doi.org/10.1016/j.apcatb.2015.05.008
0926-3373/

modified ZnO nanotube arrays was fabricated on ITO substrate and apply as PEC electrodes, the photocurrent density and the calculated theoretical efficiency for hydrogen production of the samples were evaluated to be up to 5.08 mA cm^{-2} and 5.76%, respectively. It is founded that the excellent performance is ascribed to the enhanced absorption efficiency, high speed of photo-induced charges transmission velocity and appropriate energy gap of coupled nanostructures. This study provides a promising low-cost method in the development of ternary absorber modified ZnO-based PEC electodes for water splitting system.

2. Experimental

2.1. Preparation of ZnO nanorod arrays

The preparation of ZnO nanorod arrays involves substrate pre-treatment and hydrothermal deposition. The ITO substrates ultrasonically rinsed for 30 min in acetone, isopropyl alcohol and ethanol absolution, respectively. A seed layer was firstly deposited on ITO by a dip-coating method, after heat treatment in muffle furnace at 400 °C for 1 h, followed by the incubation in the mixed solution of 0.05 M zinc nitrate hexahydrate ($Zn(NO_3)_2{\cdot}6H_2O$) and 0.05 M hexamethylenetetramine (HMTA) at 90 °C for 4 h. The obtained samples were subsequently washed with distilled water and finally dried in air.

2.2. Preparation of ZnO/ZnS nanotube arrays

The ZnO/ZnS nanotube arrays were prepared by a chemical etching and ion-exchange process by using ZnO nanorods as reactive templates. The ZnO nanorods were immersed in 0.1 M thiacetamide (TAA) solution at 90 °C for 7 h to form ZnO/ZnS nanotube arrays. The as-prepared products were washed using distilled water and then dried in air.

2.3. Preparation of ZnO/$AgSbS_2$ nanotube arrays

The ZnO/$AgSbS_2$ nanotube arrays were prepared by means of a two-stage ion-exchange process. First, Ag_2S shell was grown around the ZnO core. Second, Sb_2S_3 shell was grown on the Ag_2S. The double layer Ag_2S/Sb_2S_3 was transformed into the $AgSbS_2$ by heating the sample to 300 °C in air for 30 min.

For the growth of ZnO/Ag_2S naonotube arrays process, 4 mg of siliver nitrate ($AgNO_3$) was dissolved in 25 mL deionized water, and the ZnO/ZnS naonotube arrays was immersed in the $AgNO_3$ solution and kept for 20 min at 28 °C. For the coating of Sb_2S_3 shell, 6 mg antimony trichloride ($SbCl_3$) was dissolved in 25 mL absolute ethanol, and the ZnO/Ag_2S nanotube arrays were immersed in the $SbCl_3$ solution kept at 35 °C for 2 h. The large difference in solubility product constant of ZnS, Ag_2S and Sb_2S_3 leading to the ZnO/Ag_2S/Sb_2S_3 can be formed adopt ion-exchange process. Finally, the samples of ZnO/$AgSbS_2$ were washed with deionized water and dried in air.

2.4. Characterization

Morphology and structure of the samples was observed by HITACHI S-4800I field emission scanning electron microscope (FE-SEM) and HITACHI H-7650 transmission electron microscopy (TEM) operated at an accelerating voltage of 100 kV. X-ray diffraction (XRD) patterns of the films were performed using a Rigaku D/max-2500 using Cu Kα radiation (λ = 0.154059 nm). Optical absorption spectrums of the samples were examined by DU-8B UV/vis double-beam spectrophotometer. The calculated efficiencies of hydrogen generation (η) of the ZnO/$AgSbS_2$ nanotube arrays were estimated using the following equation [27]:

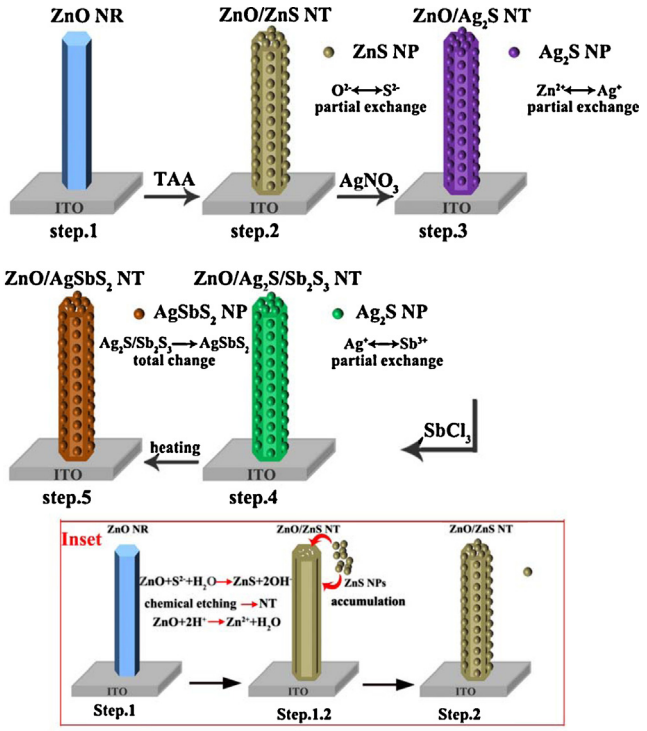

Fig. 1. Schematic illustration for the synthesis ZnO/$AgSbS_2$ nanotube arrays step by step; Inset shows: synthesis process of ZnO/ZnS NT arrays (Step.1–Step.2).

$$\eta = \left[\frac{I(1.23 - E_{bias})}{J_{light}}\right] \times 100\% \quad (1)$$

where I is the photocurrent density (mA cm^{-2}), 1.23 is the standard reduction potential of water formation from hydrogen and oxygen, E_{bias} is the applied external potential and J_{light} is the intensity of the solar simulated incident light (100 mW cm^{-2}).

3. Results and discussion

In this work, miargyrite $AgSbS_2$ modified ZnO nanotube arrays were successfully fabricated on ITO substrates through a facile hydrothermal chemical method, and the preparation process is schematically illustrated in Fig. 1. First of all, large-scale orderly hexagonal ZnO NR arrays were fabricated on ITO by a simple hydrothermal process (Step.1). In this step, a seed layer of ZnO was coated on ITO substrate after heat treating, on which seed layer would develop into ZnO NR arrays in the growth solution. It should be noted that the chemical conversion method based on ion-exchange would take place spontaneously when there are sufficient differences in the solubility products constants (K_{sp}) between the reactants and the products [28–31]. Therefore, when the ITO coated with ZnO NR arrays is immersed into 0.1 M TAA solution, the sulfidation based on ion-change will occur due to large difference between the solubility product constants (K_{sp}) of ZnO (6.8×10^{-17}) and ZnS (2.93×10^{-25}) (Eqs. (2)–(4)).

$$CH_3CSNH_2 + H_2O \rightarrow CH_3CONH_2 + H_2S \quad (2)$$

$$H_2S \rightarrow 2H^+ + S^{2-} \quad (3)$$

$$ZnO + S^{2-} + H_2O \rightarrow ZnS + 2OH^- \quad (4)$$

The further reaction of ZnO with H_2S around the surface leads to the ZnO/ZnS core/shell nanostructures (Step.2). Meanwhile, when the ZnO NR arrays were immersed in 0.1 M TAA solution, the NR

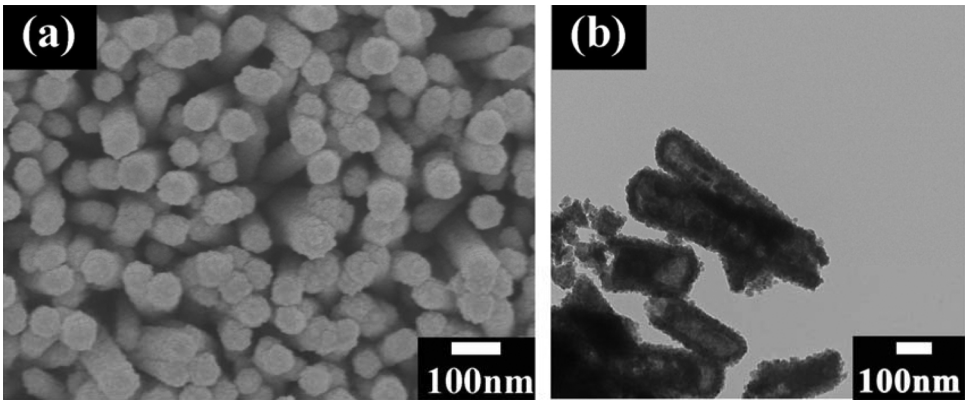

Fig. 2. SEM image (a) and TEM image (b) of ZnO/ZnS nanotubes.

will transformed into ZnO/ZnS NT, and the preparation process of NT is display in the inset of Fig. 1, which is ascribed to high concentrations of TAA solution can generate abundant H^+. As a result, the reaction solution became acid solution, ZnO NR arrays would react with H^+ in acid solution and the products are soluble salts. For the reaction process, the etching is selective and mainly focused on of top surface of ZnO due to the polar plane (0 0 2) of ZnO with high surface energy is instable, and the lateral planes parallel to *c*-axis are the most stable planes with a lower surface energy. Hence, the reaction rate of top surface is faster than that of lateral surface [32]. Finally, the ZnO/ZnS NT arrays were obtained (inset of Fig. 1). Fig. 2(a) shows the SEM image of ZnO/ZnS nanoarrays, it can be seen that the ITO substrate is covered with a large-scale highly ordered ZnO/ZnS nanoarrays, which are dense and uniform over the entire area. And the Fig. 2(b) displays the TEM image of ZnO/ZnS NT, ZnO/ZnS NT with thin-wall can be observed, and the surface looks like accumulation of a layer of nanoparticles. Afterwards, Ag_2S was formed by ion-exchange process of Zn^{2+} and Ag^+ due to large differences in K_{sp} between ZnS (2.93×10^{-25}) and Ag_2S (1.6×10^{-49}) (Eq. (5)).

$$ZnS + 2Ag^+ \rightarrow Ag_2S + Zn^{2+} \quad (5)$$

In this step, the ZnO/ZnS NT arrays converted to ZnO/Ag_2S NT arrays (Step.3). In Step.4, Ag_2S is partially converted to Sb_2S_3 shell via metal cation exchange process because of the large differences in K_{sp} between Ag_2S (1.6×10^{-49}) and Sb_2S_3 (2.9×10^{-59}), and thus the ZnO/Ag_2S/Sb_2S_3 nanotube arrays were prepared successfully. Finally, the heating treatment transformed the Ag_2S/Sb_2S_3 shell into the $AgSbS_2$ phase, and the samples of ZnO/$AgSbS_2$ nanotube arrays were obtained.

The composition and crystallographic structure of the ZnO NR arrays, ZnO/ZnS NT arrays and ZnO/$AgSbS_2$ NT arrays were characterized by X-ray diffraction (XRD). As shown in Fig. 3(a), in comparison with the standard ZnO diffraction pattern (JCPDS no. 36–1451), it can be seen that the as-prepared ZnO NRs were mainly grown along the (002) direction, in other words, the ZnO NR arrays were vertically grew on the ITO substrate. Fig. 3(b) displays XRD pattern of ZnO/ZnS nanotube arrays, in addition to ZnO, characteristic peak of ZnS can be observed, in comparison with the standard ZnS diffraction pattern (JCPDS no.12–0688), which demonstrating that the ZnO nanoarrays were converted to ZnO/ZnS nanoarrays already. The XRD pattern of ZnO/$AgSbS_2$ NT arrays is given in Fig. 3(c), in addition to ZnO and ZnS, characteristic peaks of miargyrite $AgSbS_2$ (JCPDS no. 19–1137) appear, implying that the ZnO has been converted to ZnO/$AgSbS_2$ nanoarrays. To further analyze the chemical composition of sample of ZnO/$AgSbS_2$, the element composition of sample was determined by energy dispersive spectrometer (EDS). As displayed in Fig. 4, all the peaks of Zn, O, Ag, Sb and S can be clearly observed, while the other peaks are originated from ITO glass, indicating that the product was consisted of Zn, O, Ag, Sb and S elements. The XRD pattern and EDS spectrum give the convincing evidences that ZnO/$AgSbS_2$ nanoarrays were fabricated successfully.

Furthermore, in order to investigate the bonding state and composition of ZnO/$AgSbS_2$ nanostructure, XPS measurements were taken. The survey spectrum of the ZnO/$AgSbS_2$ nanostructure is shown in Fig. 5(a). The full XPS scan form 0 to 1250 eV demonstrated that the elements Zn, O, Ag, Sb and S were existed in this sample, and the standard C 1s peak at 284.6 eV was used as a reference to correct the peak shifts. Fig. 5(b) exhibits the high-resolution XPS spectrum of Ag 3d. The peaks at 374.2 eV and 368.2 eV are assigned to the binding energy of Ag $3d_{3/2}$ and Ag $3d_{5/2}$, respectively, implying the existence of Ag^+. Fig. 5(c) shows the high-resolution XPS spectrum of Sb 3d, the peaks at 537.6 eV and 528.2 eV can be assigned to the binding energies of Sb $3d_{3/2}$ and Sb $3d_{5/2}$, respectively, indicating the existence of Sb^{3+}. Fig. 5(d) displays the high-resolution XPS spectrum of S 2p. The two peaks

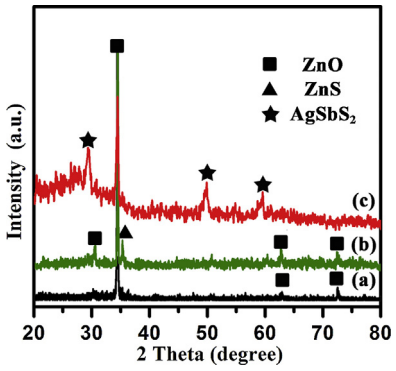

Fig. 3. XRD patterns of ZnO nanorod arrays (a), ZnO/ZnS nanotube arrays (b) and ZnO/$AgSbS_2$ nanotube arrays (c).

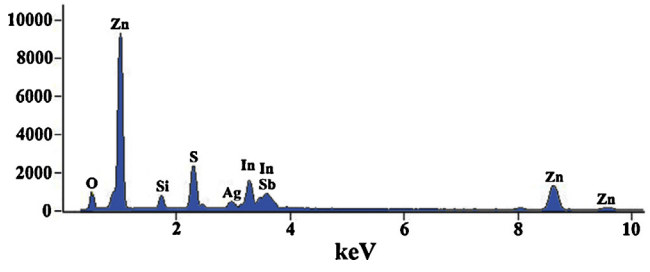

Fig. 4. EDS patterns of the ZnO/$AgSbS_2$ nanotube arrays.

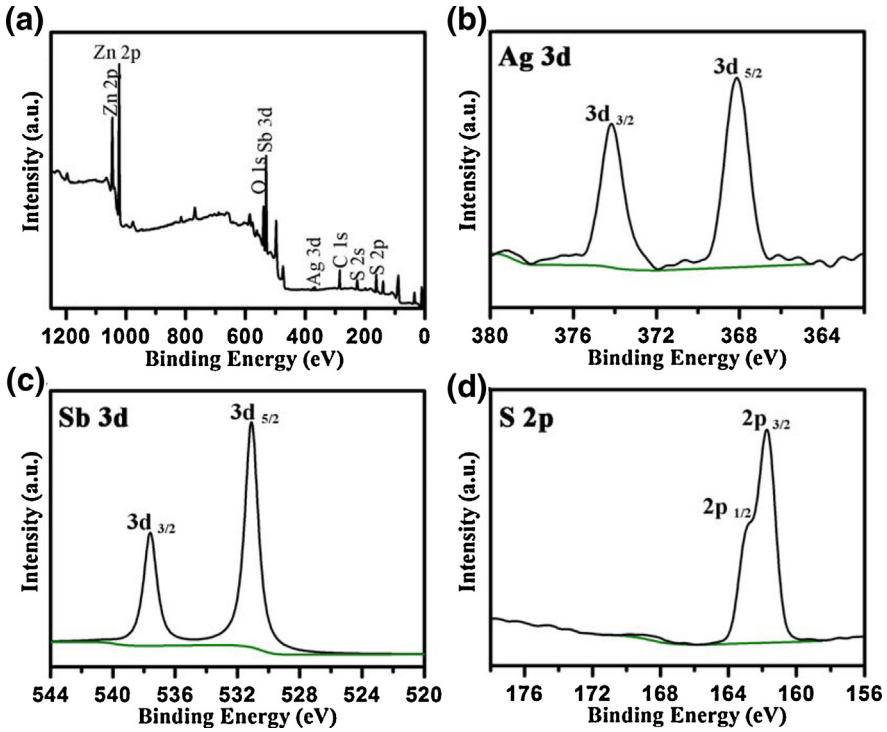

Fig. 5. XPS spectra of the as-prepared ZnO/$AgSbS_2$ nanoarrays film: (a) survey spectra, (b) high-resolution spectra of Ag 3d, (c) high-resolution spectra of Sb 3d and (d) high-resolution spectra of S 2p.

of 162.6 eV and 161.4 eV are assigned to the binding energy of S $2p_{1/2}$ and $2p_{3/2}$, respectively, indicating the existence of S^{2-}. The XPS results show that the element ratio of Zn, O, Ag, Sb and S in the ZnO/$AgSbS_2$ nanoarrays film is about 3.21:3.16:0.88:0.93:1.82 (23.15%, 22.81%, 6.37%, 6.70%, 13.12%, respectively), and the element ratio of C is about 27.85%. Therefore, the content of $AgSbS_2$ on the ZnO/$AgSbS_2$ nanoarrays film is about 21.6%. From the bonding state and composition detection results above, it can concluded that the ZnO/$AgSbS_2$ were prepared successfully. The XPS spectra, together with the XRD and EDS data, strongly support the successful preparation of ZnO/$AgSbS_2$ nanostructure based on hydrothermal chemical process.

The morphology of as-prepared products was determined by Field Emission- Scanning Electron Microscope (FE-SEM), typical SEM image and side-view SEM image of as-prepared ZnO/$AgSbS_2$ NT arrays are displayed in Fig. 6. From the Fig. 6(a), it can be seen that large-scale arrays of highly ordered ZnO/$AgSbS_2$ NT was vertically grown on the ITO substrates, implying that the hydrothermal chemical reaction based on ion-exchange is suited to obtain uniform morphology without destroying the original backbone. The inset of Fig. 6(a) shows the large-view SEM image of ZnO/$AgSbS_2$ nanoarrays, it can be seen that the NTs were covered up because of some nanoparticles accumulated on the orifice of NTs, and the NTs show a hexagonal shape with a diameter of ~120 nm. Fig. 6(b) displays the side-view SEM image of ZnO/$AgSbS_2$ nanoarrays, the length of nanoarray is measured to be approximately 1.3–1.4 μm. It can be seen that the surface and the length of nanoarrays are relatively smooth and uniform, and a layer of nanoparticles were accumulation around the nanotube surface.

The nanostructures of NTs were characterized by Transmission Electron Microscopy (TEM). Fig. 7 (a) presents a TEM image of ZnO/$AgSbS_2$ NTs at low magnification, it can be seen that the NTs were composed of uniform hollow structure with double layers, and some nanoparticles were accumulated around the outside surface of NTs. Meanwhile, the diameter and morphology of NTs is identifying with the SEM images. In order to investigate the intrinsic crystal structure of ZnO/$AgSbS_2$ NT, high resolution TEM (HRTEM) and selected-area electron diffraction (SAED) were characterized. The HRTEM image of ZnO/$AgSbS_2$ is displayed in Fig. 7(b), the sets of lattice fringes of 0.305 nm and 0.180 nm matches well to miargyrite $AgSbS_2$, the sets of lattice fringes of 0.260 nm assigned to wurtzite ZnO. The inset of Fig. 7(b) displays the SAED patterns of the ZnO/$AgSbS_2$ NTs, the obvious diffraction spots within these rings demonstrate reasonable crystallinity of the ZnO/$AgSbS_2$ is continuous polycrystalline with good crystallinity. The TEM image and HRTEM image reveal that the microstructure and composition of ZnO/$AgSbS_2$ NTs, and further prove that ZnO/$AgSbS_2$ NTs were fabricated successfully, in which ZnO is the core, and $AgSbS_2$ is the shell with the distribution of $AgSbS_2$ nanoparticles covered the top and lateral surface of NTs uniformly.

The optical performance of ZnO NR arrays and ZnO/$AgSbS_2$ NT arrays was determined by the UV-vis absorption spectra, which are displayed in Fig. 8. As shown in Fig. 8(a), the absorption of ZnO NRs films mainly focusing on the UV region because of their wide bandgap. In contrast with ZnO NRs films, $AgSbS_2$ modified ZnO NTs films exhibit an outstanding red-shift, implying that a remarkable enhancement in visible light region. Fig. 8(b) shows transmittance spectra of ZnO NRs films and ZnO/$AgSbS_2$ NTs films, it can be seen that the ZnO films shows high transmittance in the visible region and broad transmittance region. Compared with the transmittance spectra of ZnO films, the $AgSbS_2$ modified ZnO films show a lower transmittance in the visible region and narrower transmittance region, which indicate that ZnO/$AgSbS_2$ NTs films achieve the best efficiency of light absorption, and thus the PEC properties of products were enhanced significantly. It can be concluded that the $AgSbS_2$ shell could extend the photoresponse spectrum to visible region and the photo absorption was enhanced. It is because of the ideal band gap (1.72 eV) and the high optical absorption coefficient of $AgSbS_2$.

Fig.9 shows the Polt of $(OD.h\upsilon)^2$ versus $h\upsilon$ of ZnO and ZnO/$AgSbS_2$, the approximate band gap value of ZnO and ZnO/$AgSbS_2$ are determined to be ~3.04 eV and ~2.14 eV, implying

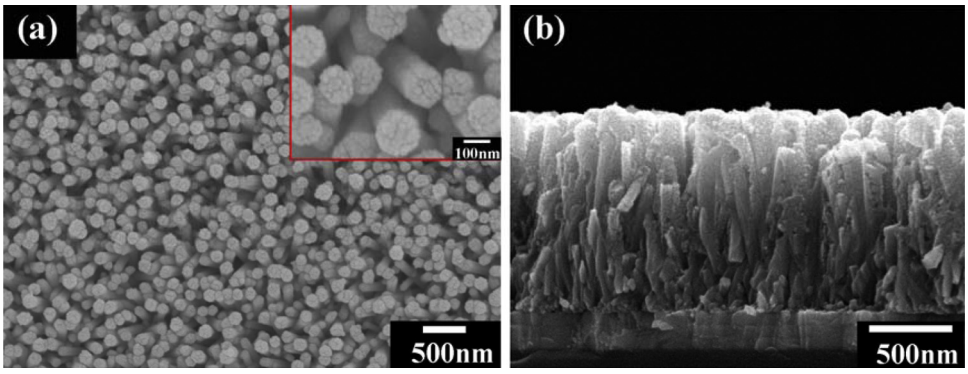

Fig. 6. Top-view SEM image (a) and side-view SEM image (b) of ZnO/$AgSbS_2$ nanoarrays;Inset of (a): large-view SEM image of ZnO/$AgSbS_2$ nanoarrays.

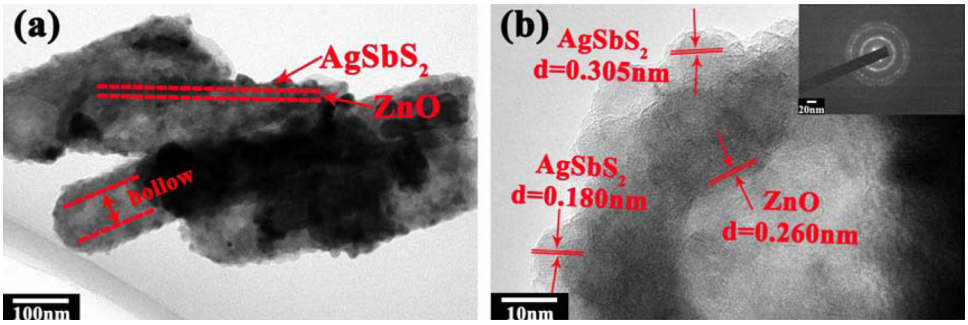

Fig. 7. TEM image (a) and HRTEM image (b) of ZnO/$AgSbS_2$; Inset shows SAED of ZnO/$AgSbS_2$.

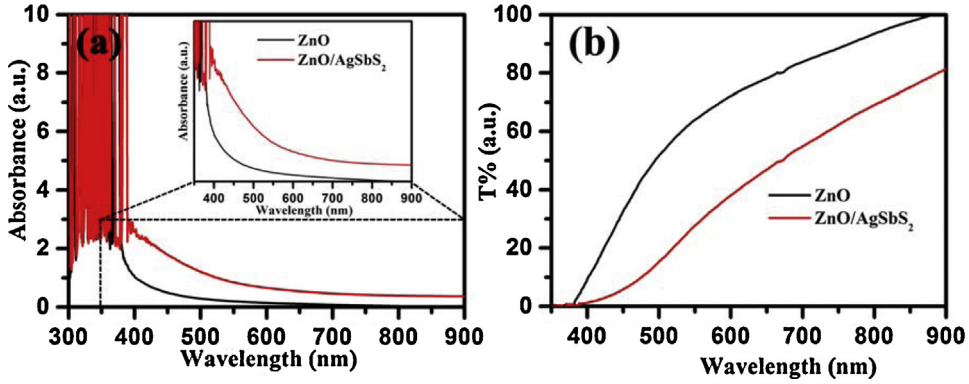

Fig. 8. UV–vis light absorption spectra (a) and transmittance spectra (b) of ZnO and ZnO/$AgSbS_2$.

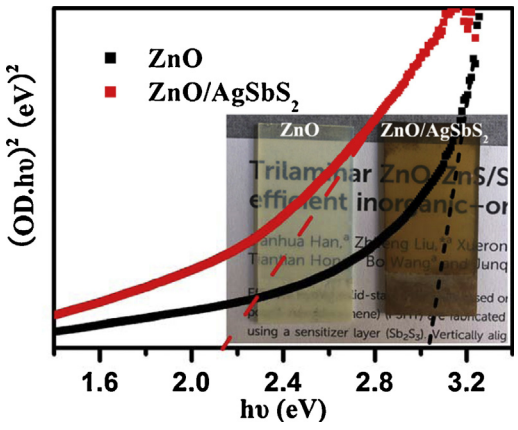

Fig. 9. Polt of $(OD.h\upsilon)^2$ versus hυ of ZnO and ZnO/$AgSbS_2$. Inset of (b) shows the photographs of ZnO and ZnO/$AgSbS_2$.

that the $AgSbS_2$ modified ZnO NTs films are suited to improve visible light absorption than that of the single ZnO NR films. Therefore, the $AgSbS_2$ modified ZnO broaden the photo response spectrum significantly than single ZnO, owing to the ideal band gap and high optical absorption coefficient of $AgSbS_2$. Therefore, the band gap of coupled ZnO/$AgSbS_2$ obtained an appropriate energy band gap. Inset of Fig.9 shows the photographs of ZnO and ZnO/$AgSbS_2$, it can be seen that after the hydrothermal chemical reaction, the color of product changes obviously, indicating that $AgSbS_2$ was covered on the surface of ZnO nanoarrays.

The as-obtained ZnO NR arrays and ZnO/$AgSbS_2$ NT arrays were applied for PEC system to assess their properties, and the photocurrent density of samples were determined by a three electrodes PEC system. The samples were operated in 1 M sodium sulphide (Na_2S) solution under irradiation of a xenon lamp with 100 mW cm^{-2}. Fig.10(a) shows the photocurrent density versus applied potential characteristics ZnO NR arrays and ZnO/$AgSbS_2$ NT arrays. It can be seen that the photocurrent densities of ZnO NR arrays

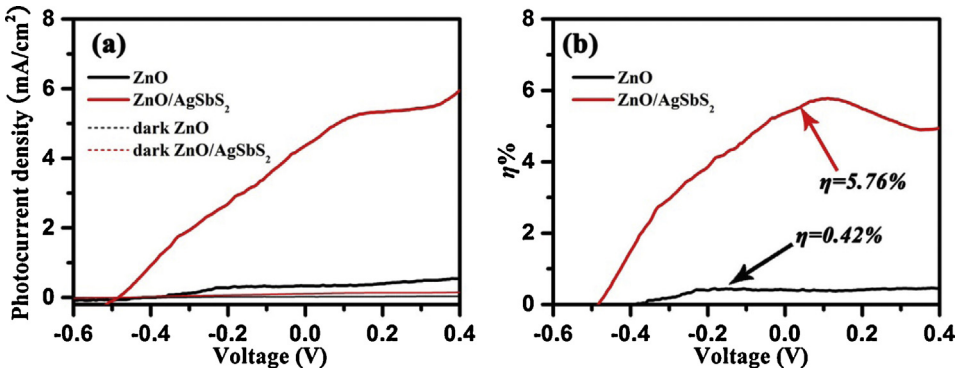

Fig. 10. Photocurrent density–voltage curves under the irradiation with 100 mW cm^{-2} and dark condition (a) and photoconversion efficiency curves (b) of ZnO and ZnO/$AgSbS_2$.

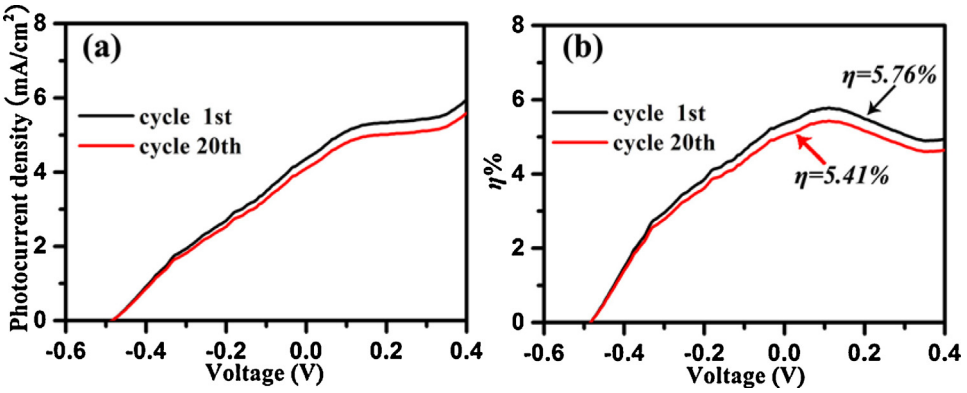

Fig. 11. Linear sweep voltammograms of cycle times (a) and photoconversion efficiency curves (b) of ZnO and ZnO/$AgSbS_2$.

Table 1
The photocurrent density calculated efficiencies of hydrogen generation of ZnO nanorod arrays and ZnO/$AgSbS_2$ nanotube arrays.

Photoelectrode	E_{bias}	I (mA/cm^2)	η (%)
ZnO	0.212	0.41	0.42
ZnO/$AgSbS_2$	0.096	5.08	5.76

and ZnO/$AgSbS_2$ NT arrays were 0.41 mA cm^{-2} at 0.212 V versus Ag/AgCl and 5.08 mA cm^{-2} at 0.096 V versus Ag/AgCl, respectively. The PEC electrodes of $AgSbS_2$ modified ZnO NT arrays achieved much higher photocurrent density than PEC electrode of ZnO NR arrays, indicating that the ZnO/$AgSbS_2$ NT arrays are more effective structures for PEC water splitting. The PEC properties of samples were further evaluated by calculating the hydrogen generation efficiencies (the calculated efficiencies of hydrogen generation of samples are displayed in the Fig. 10(b) and Table1. The supreme calculated hydrogen production efficiency value of sample was 5.76% for ZnO/$AgSbS_2$ NT arrays, the value presents a notable enhancement in comparison with single ZnO NR arrays. It can be concluded that the PEC electrodes of $AgSbS_2$ modified ZnO NT arrays is suitable for water splitting.

To further investigate the stability of ZnO/$AgSbS_2$ NT arrays PEC electrodes, linear sweep voltammograms was texted after C–V scanning for 1 and 20 cycles under illumination with 100 mW cm^{-2}, using ZnO NR arrays and ZnO/$AgSbS_2$ NT arrays as typical photoelectrode, and the photocurrent density of samples were shown in Fig.11(a). The photocurrent densities of ZnO/$AgSbS_2$ NT arrays cycle 1st and 20th were 5.08 mA cm^{-2} and 4.77 mA cm^{-2} versus Ag/AgCl, respectively. Fig.11(b) the calculated efficiencies of hydrogen generation of samples, it can be seen that the PEC electrodes of $AgSbS_2$ modified ZnO NT arrays shows much more stable current density after C–V scanning under illumination for 20 cycles, implying outstanding capability to resist photocorrosion.

It should be noted that photo response region, electrons transmission velocity and stability of core nanomaterials are three key factors determining the PEC water splitting performance. For structure of ZnO/$AgSbS_2$, an appropriate energy band gap of coupled nanostructures can be obtained by modified with the miargyrite $AgSbS_2$, and thus the photo response spectrum was broadened. As a result, the light absorption efficiency of ZnO/$AgSbS_2$ was enhanced significantly, which is conductive to PEC water splitting. It is well known that the 1D nanostructure (nanotube) without crystal boundary resistance have an extremely high-speed photo-induced charges transmission and low electrons/holes recombination, which is because of 1D nanotube can provide direct electric pathways ensure rapid collect carriers. To investigate the photo-induced charges transmission velocity of ZnO nanoarrays and ZnO/$AgSbS_2$ nanoarrays, the electrochemical impedance spectroscopy (EIS) were determined using electrochemical workstation. As we all know, the charges lifetime is related to the recombination resistance, whereas the large semicircle radius of EIS curves means large electrons and holes recombination resistance. That is, the semicircle radius reflects the electron lifetimes [33–34]. Fig. 12 shows the EIS spectroscopy of ZnO nanoarrays film and ZnO/$AgSbS_2$ nanoarrays film, it can be seen that the charges lifetime of ZnO/$AgSbS_2$ is longer than that of ZnO, which is attributed to the electrons and holes recombination resistance in ZnO/$AgSbS_2$ being lower than that in ZnO nanostructure. Based on the EIS results, it can be concluded that the ZnO/$AgSbS_2$ nanostructure is more suitable for photo-induced electrons transmission. Large-scale 1D ZnO/$AgSbS_2$ core/shell NT arrays were fabricated on ITO substrate successfully, and thus this nanostructure is suitable for charges transmission, therefore, the electrons transmission properties of

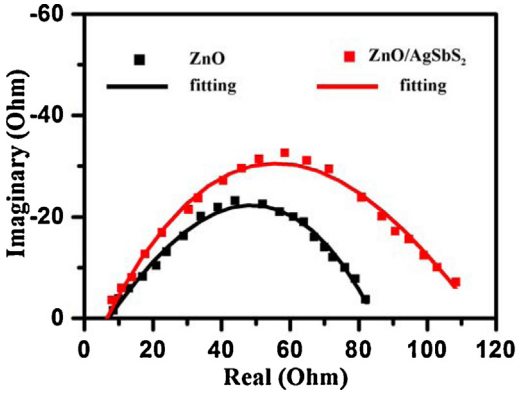

Fig. 12. Electrochemical impedance spectroscopy of ZnO nanoarrays film and $ZnO/AgSbS_2$ nanoarrays film.

$ZnO/AgSbS_2$ electrodes was improved distinctly. Meanwhile, as an amphoteric metal oxide, the instability of ZnO can be ameliorated by construct $ZnO/AgSbS_2$ core/shell nanotubes. Consequently, the electrodes of $ZnO/AgSbS_2$ nanoarrays films show excellent PEC performance .

In spite of rarely reported to date, ternary sensitizer modified metal oxide nanoarrays would be widely developed as photoelectrodes in the future due to their outstanding photoelectric properties. The ternary sensitizer modified metal oxide nanoarrays can obtain excellent PEC properties due to: (i) ideal energy band gap of coupled nanostructures (enhanced photo response spectrum); (ii) high speed of photo-induced charges transmission velocity of one-dimension nanoarrays; (iii) the protected core nanostructure. Further studies can be concentrated on the optimization of PEC properties by means of exploiting other ternary nanomaterials with ideal bandgap and high light absorption coefficient, and as sensitizer for PEC electrodes.

4. Conclusions

Vertically aligned $AgSbS_2$ modified ZnO nanotube arrays were directly fabricated on ITO substrate using ZnO NRs as templates via a facile, versatile and low-cost hydrothermal chemical process based on ion–exchange mechanism. This preparation method is easy to be controlled and developed to uniform structure without destroying the original backbone, and it can be applied to fabricate other ternary sensitizer nanomaterial for PEC electrodes. The PEC properties were texted by the electrochemical workstation, the photocurrent density and hydrogen generation efficiency of $ZnO/AgSbS_2$ nanotube arrays PEC electrode was elevated to 5.08 mA cm^{-2} and 5.76%, respectively. The results demonstrate that $AgSbS_2$ modified ZnO NT arrays is suitable for PEC water splitting, and the PEC electrode of $ZnO/AgSbS_2$ NT arrays described here shows excellent performance. Furthermore, this work will thus be important for designing and creating ternary sensitizer modified ZnO nanoarrays as PEC electodes for hydrogen production by water splitting.

Acknowledgement

The authors gratefully acknowledge financial support from National Nature Science Foundation of China (51102174).

References

[1] S.L. Xie, X.H. Lu, T. Zhai, W. Li, M.H. Yu, C.L. Liang, Y.X. Tong, Enhanced photoactivity and stability of carbon and nitrogen co-treated ZnO nanorod arrays for photoelectrochemical water splitting, J. Mater. Chem. 22 (2012) 14272–14275.
[2] F.E. Osterloh, Inorganic nanostructures for photoelectrochemical and photocatalytic water splitting, Chem. Soc. Rev. 42 (2013) 2294–2320.
[3] X. Zhang, Y. Liu, Z.H. Kang, 3D branched ZnO nanowire arrays decorated with plasmonic Au nanoparticles for high-performance photoelectrochemical water splitting, ACS Appl. Mater. Interfaces 6 (2014) 4480–4489.
[4] S.H. Shen, L.J. Guo, X.B. Chen, F. Ren, S.S. Mao, Effect of Ag_2S on solar-driven photocatalytic hydrogen evolution of nanostructured CdS, Int. J. Hydrogen Energy 35 (2010) 7110–7115.
[5] Q. Huang, Q. Li, X.D. Xiao, Hydrogen evolution from Pt nanoparticles covered *p*-type CdS:Cu photocathode in scavenger-free electrolyte, J. Phys. Chem. C 118 (2014) 2306–2311.
[6] Z.H. Zhang, L.B. Zhang, M.N. Hedhili, H.N. Zhang, P. Wang, Plasmonic gold nanocrystals coupled with photonic crystal seamlessly on TiO_2 nanotube photoelectrodes for efficient visible light photoelectrochemical water splitting, Nano Lett. 13 (2013) 14–20.
[7] Y.X. Li, J.X. Wang, S.Q. Peng, G.X. Lu, S.B. Li, Photocatalytic hydrogen generation in the presence of glucose over ZnS-coated ZnIn2S4 under visible light irradiation, Int. J. Hydrogen Energy 35 (2010) 7116–7126.
[8] Y.X. Li, J. Du, S.Q. Peng, D. Xie, G.X. Lu, S.B. Li, Enhancement of photocatalytic activity of cadmium sulfide for hydrogen evolution by photoetching, Int. J. Hydrogen Energy 33 (2008) 2007–2013.
[9] Y.B. Li, Z.F. Liu, Y. Wang, Z.C. Liu, J.H. Han, J. Ya, ZnO/CuInS2 core/shell heterojunction nanoarry for photoelectrochemical water splitting, Int. J. Hydrogen Energy 37 (2012) 15029–15037.
[10] A. Fujishima, K. Honda, Electrochemical photolysis of water at a semiconductor electrode, Nature 238 (1972) 37–38.
[11] G.M. Wang, H.Y. Wang, Y.C. Ling, Y.C. Tang, X.Y. Yang, R.C. Fitzmorris, C.C. Wang, J.Z. Zhang, Y. Li, Hydrogen-treated TiO_2 nanowire arrays for photoelectrochemical water splitting, Nano Lett. 11 (2011) 3026–3033.
[12] K.F. Liu, W.B. Wu, B.L. Chen, X.D. Chen, N.N. Zhang, Continuous growth and improved PL property of ZnO nanoarrays with assistance, Nanoscale 5 (2013) 5986–5990.
[13] A.A. Tahir, K.G.U. Wijayantha, S. Saremi-Yarahmadi, M. Mazhar, V. Mckee, Nanostructured α-Fe_2O_3 thin films for photoelectrochemical hydrogen generation, Chem. Mater. 21 (2009) 3763–3772.
[14] X.B. Chen, L. Liu, P.Y. Yu, S.S. Mao, Increasing solar absorption for photocatalysis with black hydrogenated titanium dioxide nanocrystals, Science 331 (2011) 746–750.
[15] Q.F. Zhang, T.P. Chou, B. Russo, S.A. Jenekhe, G.Z. Cao, Polydisperse aggregates of ZnO nanocrystallites: a method for energy-conversion-efficiency enhancement in dye-sensitized solar cells, Adv. Funct. Mater. 18 (2008) 1654–1660.
[16] M. McCune, W. Zhang, Y.L. Deng, High efficiency dye-sensitized solar cells based on three-dimensional multilayered ZnO nanowire arrays with caterpillar-like structure, Nano Lett. 12 (2012) 3656–3662.
[17] D.J. Gargas, H.W. Gao, H. Wang, P.D. Yang, High quantum efficiency of band-edge emission from ZnO nanowire, Nano Lett. 11 (2011) 3792–3796.
[18] G.W. She, X.H. Zhang, W.S. Shi, X. Fan, J.C. Chang, C.S. Lee, S.T. Lee, C.H. Liu, Controlled synthesis of oriented single-crystal ZnO nanotube arrays on transparent conductive substrates, Appl. Phys. Lett. 92 (2008) 053111.
[19] J.J. Qiu, X.M. Li, W.Z. He, S.J. Park, H.K. Kim, Y.H. Hwang, J.H. Lee, Y.D. Kim, The growth mechanism and optical properties of ultralong ZnO nanorod arrays with a high aspect ratio by a preheating hydrothermal method, Nanotechnology 20 (2009) 155603.
[20] M. Law, L.E. Greene, J.C. Johnson, R. Saykally, P.D. Yang, Nanowire dye-sensitized solar cells, Nat. Mater. 4 (2005) 455–459.
[21] B.M. Wen, Y.Z. Huang, J.J. Boland, Controllable growth of ZnO nanostructures by a simple solvothermal process, J. Phys. Chem. C 112 (2008) 106–111.
[22] S. Khanchandani, S. Kundu, A. Patra, A.K. Ganguli, Shell thickness dependent photocatalyic properties of ZnO/CdS core–shell nanorods, J. Phys. Chem. C 116 (2012) 23653–23662.
[23] X.N. Wang, H.J. Zhu, Y.M. Xu, H. Wang, Y. Tao, S.K. Hark, X.D. Xiao, Q. Li, Aligned ZnO/CdTe core-shell nanocable arrays on indium tin oxide: synthesis and photoelectrochemical properties, ACS Nano 4 (2010) 3302–3308.
[24] C.C. Liu, Z.F. Liu, J.W. Li, J.H. Han, Y. Wang, Z.C. Liu, J. Ya, Cu-doping ZnO/ZnS nanorods serve as the photoanode to enhance photocurrent and conversion efficiency, Microelectron. Eng. 103 (2013) 12–16.
[25] M.J. Capistrán, M.T.S. Nair, P.K. Nair, Antimony sulfide and silver antimony sulfide absorbers for thin film solar cells, MRS Proceedings (2012) 1447, mrss 12-1447 - v07-v11.
[26] Y.R. Ho, M.W. Lee, AgSbS2 semiconductor-sensitized solar cells, Electrochem. Commun. 26 (2013) 48–51.
[27] M.G. Walter, E.L. Warren, J.R. Mckone, S.W. Boettcher, Q.X. Mi, E.A. Santori, N.S. Lewis, Solar water splitting cells, Chem. Rev. 110 (2010) 6446–6473.
[28] J.H. Han, Z.F. Liu, X.R. Zheng, K.Y. Guo, X.Q. Zhang, T.T. Hong, B. Wang, J.Q. Liu, Trilaminar ZnO/ZnS/Sb2S3 nanotube arrays for efficient inorganic–organic hybrid solar cells, RSC Adv. 4 (2014) 23807–23814.
[29] Q. Xiang, B. Cheng, J. Yu, Hierarchical porous CdS nanosheet-assembled flowers with enhanced visible-light photocatalytic H2-production performance, Appl. Catal. B: Environ. 138–139 (2013) 299–303.
[30] N. Bao, L. Shen, T. Takata, K. Domen, Self-templated synthesis of nanoporous CdS nanostructures for highly efficient photocatalytic hydrogen under visible light, Chem. Mater. 20 (1) (2008) 110–117.
[31] D. Lang, F. Liu, G. Qiu, X. Feng, Q. Xiang, Synthesis and visible-light photocatalytic performance of cadmium sulfide and oxide hexagonal nanoplates, ChemPlusChem 79 (12) (2014) 1726–1732.

[32] Z.F. Liu, C.C. Liu, J. Ya, L. E, Controlled synthesis of ZnO and TiO_2 nanotubes by chemical method and their application in dye-sensitized solar cells, Renewable Energy 36 (2011) 1177–1181.
[33] W.Q. Wu, Y.F. Xu, H.S. Rao, C.Y. Su, D.B. Kuang, Multistack integration of three-dimensional hyperbranched anatase titania architectures for high-efficiency dye-sensitized solar cells, J. Am. Chem. Soc. 136 (2014) 6437–6445.
[34] S.C. Hsu, W.P. Liao, W.H. Lin, J.J. Wu, Modulation of photocarrier dynamics in indoline dye-modified TiO2 nanorod array/P3HT hybrid solar cell with 4-*tert*-butylpridine, J. Phys. Chem. C 116 (49) (2012) 25721–25726.